AGU PUBLICATIONS

JGR

Journal of Geophysical Research: Oceans

RESEARCH ARTICLE

10.1002/2014JC009957

Key Points:
- Standing waves in SCS are analyzed
- Standing wave wavelengths are ~300 km and amplitudes ~100 m
- Occurrence distributions show interannual and intraseasonal variability

Correspondence to:
Q. Zheng,
quanan@atmos.umd.edu

Citation:
Zheng, Q., J. Hu, B. Zhu, Y. Feng, Y.-H. Jo, Z. Sun, J. Zhu, H. Lin, J. Li, and Y. Xu (2014), Standing wave modes observed in the South China Sea deep basin, *J. Geophys. Res. Oceans*, *119*, doi:10.1002/2014JC009957.

Received 12 MAR 2014
Accepted 17 JUN 2014
Accepted article online 20 JUN 2014

Standing wave modes observed in the South China Sea deep basin

Quanan Zheng[1,2], Jianyu Hu[1,2], Benlu Zhu[1,3], Ying Feng[4], Young-Heon Jo[5], Zhenyu Sun[2], Jia Zhu[2], Hongyang Lin[2], Junyi Li[1,2], and Ying Xu[1,6]

[1]Department of Atmospheric and Oceanic Science, University of Maryland, College Park, Maryland, USA, [2]State Key Laboratory of Marine Environmental Science, College of Ocean and Earth Sciences, Xiamen University, Xiamen, China, [3]Fujian Marine Forecasts, Fuzhou, China, [4]The First Institute of Oceanography, State Oceanic Administration, Qingdao, China, [5]Department of Oceanography, Pusan National University, Busan, Republic of Korea, [6]National Satellite Ocean Applications Service, State Oceanic Administration, Beijing, China

Abstract This study deals with standing wave or seiche events using cruise observations, satellite altimeter data, and theoretical analysis. Cruise missions in summer 2007 and 2009 detected internal oscillation signals in the South China Sea (SCS) deep basin. The signals have average wavelengths of 320 and 390 km and the maximum amplitudes of 50–100 m at layers 500–700 m and 1500–1700 m. Satellite altimeter sea level anomaly (SLA) images and the second intrinsic mode function (IMF2) images derived from the empirical mode decomposition (EMD) analysis show that the observed internal oscillations are a portion of 2-D seiche modes, which lasted for at least 2 weeks. We recognize that the observed internal oscillation signals represent seiche modes $H_{5,3}$ and $H_{5,1}$ derived from a rectangular model ocean basin with a uniform depth, a west-east length of 1000 km and a north-south width of 800 km. Statistical analysis of standing wave modes $H_{4,0}$, $H_{5,1}$, and $H_{5,3}$ with the average wavelength of 500, 390, and 320 km indicates that from 1993 to 2012 (1045 weeks), total 94 events with total temporal coverage of 218 weeks are affirmed. The total occurrence frequency is 20.9%. Histograms of annual distributions of seiche events and timespans show an interannual variability of about 9 years, with peak years 1993, 1994, 1998, 2001, and 2011. While monthly distributions show an intraseasonal variability double-peaked in May and October, transit periods of East Asia monsoon in the SCS.

1. Introduction

Previous investigators have found that a standing wave phenomenon may occur in an enclosed or semienclosed body of water, and termed the phenomenon "seiches" [*Lamb*, 1945; *Raichlen*, 1966; *Wilson*, 1972; *Mei*, 1992; *Rabinovich*, 2009]. *Toshiyuki and Kajiura* [1982] observed seiche-induced sea surface level displacement as high as 2.78 m in the Nagasaki Bay, Japan, which is connected with the East China Sea and characterized by active seiches. *Cao et al*. [2001] analyzed 65 seiche events in the harbors along the Bohai Sea and the Yellow Sea coasts, and found that thunderstorms and squall lines are main mechanisms for formation of large-amplitude seiches. *Xia et al*. [2002] detected 327 short-period seiche events along the north coast of the SCS from the tidal gauge records from 1953 to 1994. The observed amplitudes of seiches range from 20 to 102 cm. Seiche phenomena were also observed in the Adriatic Sea [*Vilibić and Mihanović*, 2003] and the Sulu Sea [*Giese and Hollander*, 1987]. All the above-mentioned cases are categorized to the atmospherically forced seiches. Therefore, they appear as water surface seiches. For semienclosed open seas, seiches may appear as long, low-frequency standing waves. *Metzner et al*. [2000] observed seiches of wavelengths up to several hundred kilometers in the Baltic Sea.

For coastal ocean seiches, major generation mechanisms include atmospheric forcing, such as wind or atmospheric pressure gradients, and tides. Minor mechanisms include seismic disturbances such as tsunami and seismically formed ocean waves. For a semienclosed ocean basin, *Wüest and Farmer* [2003] suggested that the oscillations in connected water bodies, having a periodicity close to that of the eigen oscillation mode or one of harmonics of the basin, are an important disturbance source to initiate seiche events. A set of seiche eigen periods and associated modal structures is a fundamental property of the ocean basin, which is independent of the external forcing mechanisms. In all the cases, seiches are generated if and only

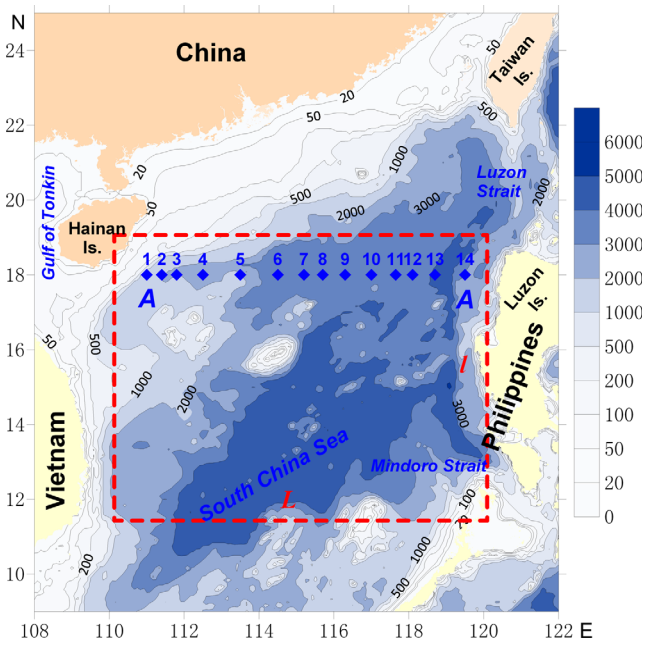

Figure 1. A chart of the SCS deep basin. Blue diamonds and codes 1–14 along 18°N line *AA* show conductivity-temperature-depth (CTD) survey stations for a cruise mission from 20 to 24 August 2007. Red rectangle represents a model ocean basin used for calculation of eigen modes. Numerals on isobaths and color bars are in m.

if the disturbances satisfy the resonant conditions with the ocean basin, i.e., the periods or wavelengths of the disturbances are the same as or very close to the resonant periods or wavelengths of eigen modes of the basin.

In a vertically stratified water body, the internal waves that occur and propagate in water are a common phenomenon [*Wüest and Farmer*, 2003]. Similarly to water surface seiches, it is possible for the internal waves to generate internal seiches, when the traveling internal waves and the internal waves reflected by the basin boundaries overlap each other and form standing waves. *Münnich et al.* [1992] observed such internal seiches in an alpine lake.

The South China Sea (SCS) is a large marginal sea of the west Northern Pacific Ocean (NPO), covering a water area between 2°30′N and 23°30′N and 99°10′E and 121°50′E. As shown in Figure 1, the SCS is a semienclosed ocean basin surrounded by lands or broad continental shelves on the north, west, and south sides and a generally north-south running island chain consisting of the Taiwan Island and the Philippine Islands (T-P) on the east side. There is a deep basin with a maximum depth deeper than 5500 m, lying SW-NE ward at the central and eastern SCS. On the east side, water of the SCS connects with water of the NPO through gaps of the T-P island chain. The major gaps are the Luzon Strait (LS) located between the Taiwan Island and the Luzon Island and the Mindoro Strait crossing the Philippine Islands (Figure 1). The SCS is characterized by strong stratification, energetic and active internal waves [*Ramp et al.*, 2004; *Zheng et al.*, 2007, 2008a, 2008b; *Cai et al.*, 2012] and mesoscale eddies [*Wang and Chern*, 1987; *Li et al.*, 1998; *Metzger and Hurlburt*, 2001; *Wang et al.*, 2003; *Jia and Liu*, 2004; *Wang et al.*, 2008b; *Xiu et al.*, 2010; *Hu et al.*, 2011, 2012; *Nan et al.*, 2011; *Xie et al.*, 2011; *Zheng et al.*, 2011; *Lin et al.*, 2012]. In particular, previous investigators have evidenced propagation of the Rossby waves originating from the NPO into the SCS [*White and Saur*, 1981; *Hu et al.*, 2001; *Zheng et al.*, 2011; *Hu et al.*, 2012].

The above analysis indicates that the SCS deep basin has three remarkable features: (1) semienclosed geometry, (2) strong stratification, and (3) direct connection to the NPO, a powerful, broad-bandwidth oscillation source. These three features constitute favorable dynamical conditions for generation of internal seiches. The next section analyzes the standing wave or seiche modes using a rectangular model ocean basin. Sections 3 and 4 analyze the internal seiche phenomena in the cruise data observed in the SCS deep basin in summer 2007 and 2009. Section 5 gives statistical analysis of seiche events. Sections 6 and 7 contain discussion and conclusions.

2. Standing Wave Modes

The basic theory of standing waves or seiche oscillations is similar to the theories of free and forced oscillations of mechanical, electronic, and acoustic systems. In other words, seiche oscillations in a semienclosed ocean basin have physical characteristics similar to the vibrations of a guitar string or an elastic membrane [*Rabinovich*, 2009].

For a rectangular ocean basin with a length L ($x = 0, L$), a width l ($y = 0, l$), and a uniform depth H, seiche oscillations have the form [*Lamb*, 1945; *Mei*, 1992]

Table 1. The Eigen Wavelengths (km) of the SCS Deep Basin Derived From a Rectangular Model Ocean Basin of 1000 by 800 km

$m =$	0	1	2	3	4	5	6	7	8	9	10
$n = 0$		2000	1000	667	500	400	333	288	250	222	200
1	1600	1249	848	615	477	388	326	281	247	220	198
2	800	743	625	512	424	356	308	269	239	214	194
3	533	515	471	416	365	320	283	252	226	205	187

$$\zeta_{m,n}(x,y,t)=A_{mn}\cos\frac{m\pi x}{L}\cos\frac{n\pi y}{l}\cos\omega t, \tag{1}$$

where $m, n = 0, 1, 2, \ldots$. The eigen wave numbers are

$$k_{mn}=\left[\left(\frac{m\pi}{L}\right)^2+\left(\frac{n\pi}{l}\right)^2\right]^{1/2}. \tag{2}$$

The corresponding eigen periods are [*Raichlen*, 1966]

$$T_{mn}=\frac{2}{\sqrt{gH}}\left[\left(\frac{m}{L}\right)^2+\left(\frac{n}{l}\right)^2\right]^{-1/2}, \tag{3}$$

where g is the gravitational acceleration.

The eigen wavelengths can be derived from equation (2)

$$\lambda_{mn}=2\left[\left(\frac{m}{L}\right)^2+\left(\frac{n}{l}\right)^2\right]^{-1/2}. \tag{4}$$

In the case of the SCS, we use a rectangular model ocean basin to approximately represent the SCS deep basin as shown in Figure 1. The model has a west-east length L of 1000 km, and a north-south width l of 800 km. From equation (4), we calculate a set of eigen wavelengths of seiche modes λ_{mn}. The eigen wavelengths for $m = 0, 1, 2, \ldots 10$ and $n = 0, 1, 2, 3$ are listed in Table 1. One can see that the eigen wavelength components are abundant but discrete. From the view of the sea level, the standing waves would result in alternative positive-negative sea level anomaly corresponding to the wave crest and trough. A combination of m and n represents a 2-D standing-wave-induced sea level field mode $H_{m,n}$ (see $H_{5,1}$ and $H_{5,3}$ in Figure 6).

From Figure 6, one can see that each positive (negative) sea level anomaly center is surrounded by negative (positive) sea level anomaly centers and forms an isolated high (low) sea level elevation (depression). To sustain the sea level elevation (depression), the water body must rotate anticyclonically (cyclonically), depending on the initial conditions, the background circulation and the Coriolis force, so that the sea level elevation (depression) center behaves like an anticyclonic (cyclonic) eddy.

3. Seiche Event Observed in August 2007

3.1. Cruise Observations

A hydrodynamic cruise mission was carried out by South China Sea Institute of Oceanology, Chinese Academy of Sciences in the SCS deep basin in August 2007 [*Nan et al.*, 2011]. The CTD survey was conducted along section 18°N as shown as section *AA* in Figure 1. There are 14 CTD stations coded from 1 to 14 distributed between 111°E and 119°30′E. Most distances between two adjacent stations are 0.5° longitude, except 1° longitude from station 3 to station 6 and between stations 13 and 14. The water depth is gradually getting deeper eastward from 1405 m at station 1 to 5500 m between stations 13 and 14. The data collection was done from 20 to 24 August 2007. At each station, the water temperature, salinity (conductivity), and depth (pressure) were observed at a sampling interval of 24 Hz with Seabird SBE-911 or Seabird SBE-25 conductivity, temperature and depth profiler (both from Sea-Bird Electronics, Inc.). The major specifications of the profilers are temperature accuracy 0.001°C and temperature resolution 0.0002°C, conductivity accuracy

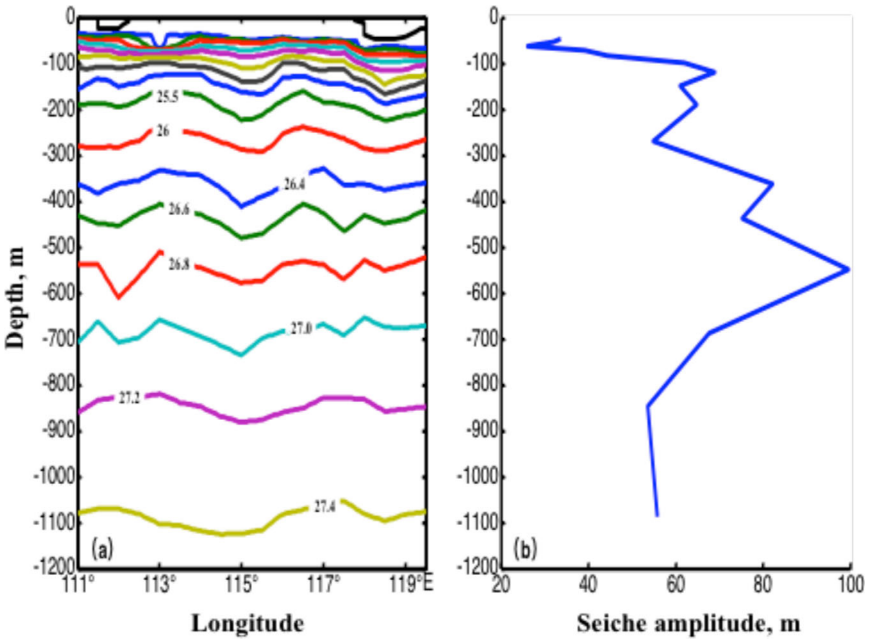

Figure 2. Vertical distributions of (a) the density (σ_θ) along section 18°N and (b) the maximum amplitudes of internal oscillation signals (peak-trough).

0.0003 S m^{-1} and resolution 0.00004 S m^{-1}, pressure accuracy 0.125 db and resolution 0.0125 db (about 1 m of the vertical resolution of raw data).

The vertical distribution of the density σ_θ calculated from measured temperature and salinity data from the sea surface to depth 1100 m as shown in Figure 2a. One can see that below 100 m down to 1100 m, there are systematical internal oscillation signals along isopycnals. We measure dominant wavelengths of the signals as 320 km from 100 to 700 m and 340 km below 850 m. Note that in a layer from 350 to 700 m the signals contain another short-wavelength component with a wavelength of about 120 km. The vertical distribution of the maximum amplitudes of internal oscillation signals (peak-trough) is shown in Figure 2b. One can see that the maximum amplitudes up to 100 m are also distributed in the 350–700 m layer. Beyond the layer, the amplitudes gradually decrease in the upper and lower layers.

Further examining Figures 2a and 2b, we find that the initial disturbance with the largest amplitude (~100 m) was first formed at 600 m near the western boundary of the deep basin (around 112°E), and appeared as a peaked leading pulse with a long oscillating tail. This disturbance signal was regulated to near monochromatic oscillations when propagating upward and downward, implying a resonant set up process of the disturbance signal with the SCS deep basin.

3.2. Interpretation of Satellite Sea Level Data

From the cruise data, we have found the internal oscillation signals and determine their oscillation source located at layer of 500–700 m. However, it is impossible to obtain the horizontal propagation features of the oscillation signals from the cruise observations of 5 days from 20 to 24 August 2007. In order to further understand the nature and the variability of the oscillations, we use satellite sea level data as a supplementary means.

Satellite altimeter sea level data used in this study are maps of absolute dynamic topography (MADT) and sea level anomaly (SLA) data from 6 January 1993 to 26 December 2012. Both data products are produced and distributed by Archiving Validation and Interpretation of Satellite Data in Oceanography (AVISO), the Centre National d'Études Spatiales (CNES) of France. MADT data are defined as the sea surface height above the geoid, thus including sea level anomaly (SLA) and mean dynamic topography (MDT). The data sets are merged products derived from TOPEX/POSEIDON (T/P), Jason-1/2 (French-US altimeter satellites), ERS-1/2 (European Remote Sensing satellites), and ENVISAT (European Remote Sensing satellite) altimeters. The gridded MADT are geophysically/meteorologically corrected (tides, ionosphere, wet and dry troposphere)

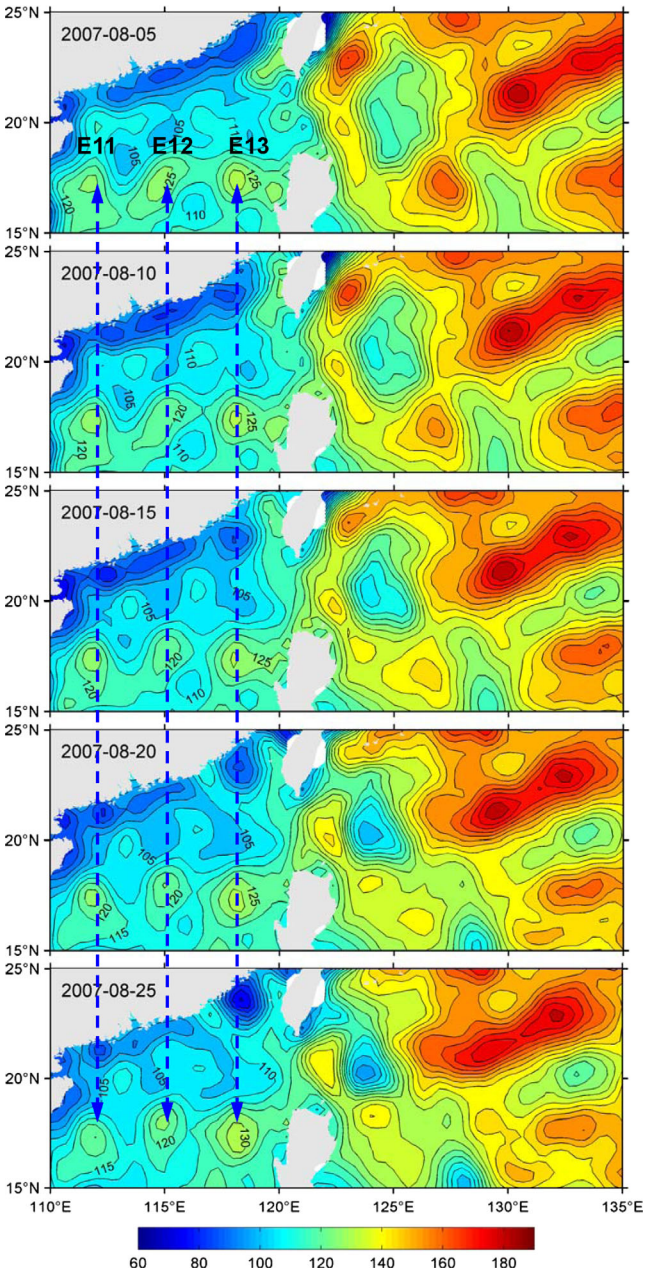

Figure 3. MADT of the north SCS and the adjacent NPO on 5, 10, 15, 20, and 25 August 2007. Three sea level elevation centers E11, E12, and E13 are distributed along around 18°N in the SCS deep basin with the average distance of 320 km. Color codes are absolute sea levels in cm.

and interpolated onto Mercator grids of 1/4° horizontal resolution with global ocean coverage except high latitude oceans. The sea level height accuracy of the products is about 2 cm.

Figure 3 shows MADT of the north SCS and the adjacent NPO of 5, 10, 15, 20, and 25 August 2007, covering the cruise mission from 20 to 24 August 2007. One can see a row of three sea level elevation centers E11, E12, and E13 distributed along around 18°N in the SCS deep basin between the mouth of the Gulf of Tonkin and the Luzon Island. The imagery patterns show the following important information: (1) E11–E13 are generally shaped of an ellipse with a length scale of about 150 km and central sea levels of 20–35 cm higher than the mean sea level; (2) E11–E13 are evenly spaced with the average distance of 320 km; and (3) the most important point is that positions of E11–E13 sustained unchanged for at least 3 weeks from 5 to 25 August 2007, in other words, they were standing there.

3.3. Correspondence of Sea Level Signatures and Internal Oscillations

In order to determine the feasibility that the SLA signatures are used to represent the internal oscillation signals, we examine the correlation relations between the two.

Figures 4a and 4b show a wave pattern comparison of the sea level along 18°N in the SCS deep basin taken from weakly SLA images on 15, 22, and 29 August 2007 to internal oscillations of isopycnals 24, 24.5, 25, 25.5, and 26 measured along the same section during the cruise mission from 20 to 24 August 2007. One can see that the two groups of wave patterns have a remarkable negative correlation relationship with a maximum correlation coefficient of -0.8 at 300 m. Further calculations of correlation coefficients versus the depth indicate that the correlation coefficients higher than -0.5 are distributed at a layer from 150 to 700 m rather than the surface layer, as shown in Figure 4c. Meanwhile, we find that the amplitude of the SLA signatures η and that of the internal oscillation signals ς satisfy an empirical relation of $\eta = (1.5\varsigma + 5.5) \times 10^{-3}$, with a correlation coefficient $R^2 = 0.99$.

The above analysis results indicate that there exist excellent wave pattern correspondence and quantitative amplitude dependence between the SLA signatures and the internal oscillation signals. This implies that it

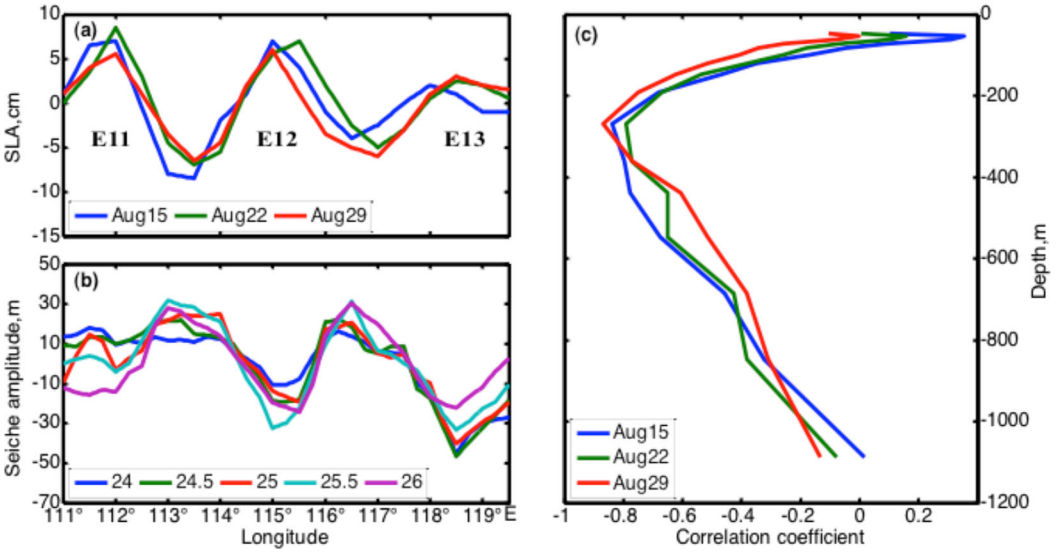

Figure 4. Comparison of SLA signatures (a) to cruise-measured internal oscillation signals of isopycnals (b) along 18°N in the SCS deep basin in August 2007, and (c) vertical distribution of correlation coefficients between the two.

is feasible to use satellite SLA data for analyzing existence, propagation, and evolution of mesoscale internal oscillations in the semienclosed SCS deep basin. Meanwhile, the above analysis results confirm that the three standing sea level elevation centers distributed along around 18°N in the SCS deep basin, which is shown in MADT time series on 5, 10, 15, 20, and 25 August 2007, were sea surface manifestations of the internal oscillation signals observed by the cruise mission from 20 to 24 August 2007. This represents an internal seiche event, which has ever been observed in the SCS deep basin.

3.4. Comparison of SLA Patterns to Seiche Modes

Sea level signatures in MADT as shown in Figure 3 contain contributions from a broad spectral band of ocean processes. However, standing wave modes may occur at specific frequencies or wavelengths. As above mentioned, the three standing sea level elevation centers in Figure 3 represent an internal standing wave train, which has an average wavelength of about 320 km. In order to compare sea level signatures of internal standing waves to 2-D seiche modes as shown in Figure 6, we extract 2-D sea level patterns of 320 km band from SLA data from 6 January 1993 to 26 December 2012 using an empirical mode decomposition (EMD) method. The method is a time-frequency (wave number) analysis technique [*Huang et al.*, 1998]. The key point of the method is that any complicated data set can be decomposed into a finite and often small number of intrinsic mode functions (IMFs) depending the nature of the data sets. The IMFs, which are determined by the signal itself but not predetermined kernels, represent the natural oscillatory mode embedded in the signal. After removing all number of IMFs from the data set, the remaining data are the local trend for the observation period. Mathematically, a time series data set $x(t)$ is decomposed in terms of IMFs, c_j, i.e.,

$$x(t)=\sum_{j=1}^{n} c_j + r_n,$$

where r_n is the trend or residue. IMFs are simple oscillatory functions with varying amplitude and frequency. The structure of each IMF is determined by the natural amplitude variations in the time series.

In order to obtain 2-D IMFs of the SCS deep basin, we apply the EMD method to decomposition of 2-D SLA images. From 2-D IMF images, we estimate that wavelengths of wave-like SLA patterns in IMF2 are within a range from 300 to 500 km, which covers that of the observed standing waves in the SCS deep basin. Figure 5 shows two cases of 2-D SLA images of IMF2 of the SCS and adjacent NPO on 29 August and 26 September 2007. One can see that regular patterns of alternate positive-negative SLA centers are distributed in the SCS deep basin enclosed by dashed lines. Figure 6 shows comparisons of the SLA patterns to standing wave modes of a uniformly deep ocean basin of 1000 by 800 km. Figure 6a shows the case of 29 August 2007,

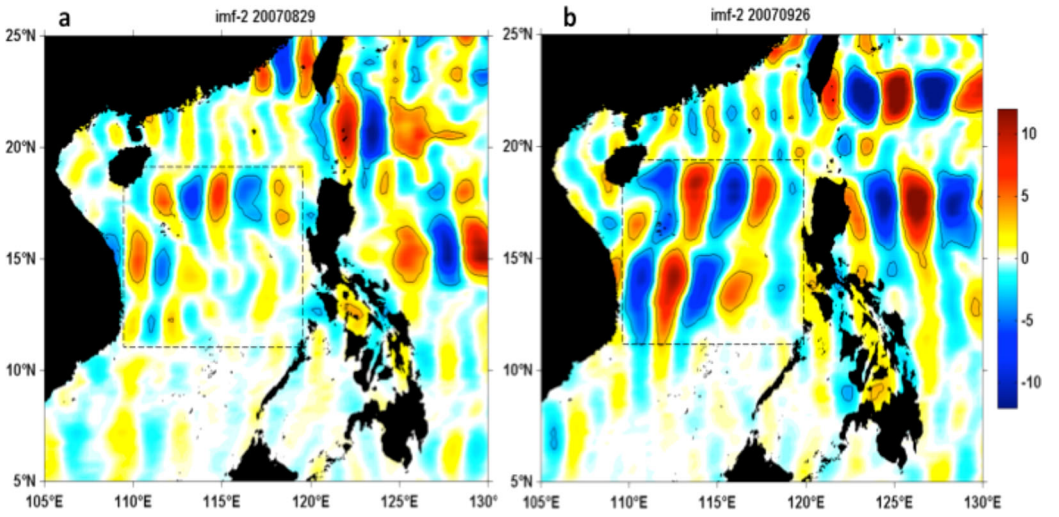

Figure 5. SLA images of IMF2 of the SCS and adjacent NPO on 29 August and 26 September 2007. Dashed-line rectangles represent the SCS deep basin defined in Figure 1. Color codes are SLA in cm.

which represents the same seiche event observed by the cruise mission from 20 to 24 August 2007 and shown in Figure 3. Figure 6b shows theoretical standing wave mode $H_{5,3}$ (for $m = 5$ and $n = 3$). The pattern similarity of Figures 6a and 6b is 75% (13.5/18). Both images show that the wavelength of standing waves is about 320 km. Figures 6c and 6d show the case of 26 September 2007, 4 weeks later of the case of 29 August. The wave patterns had evolved to theoretical standing wave mode $H_{5,1}$. The pattern similarity of Figures 6c and 6d is 87.5% (10.5/12). The wavelength of standing waves is about 390 km. The two cases indicate that the nature of standing eddy or standing wave phenomena observed in the SCS deep basin is one of intrinsic standing wave or seiche modes of the basin.

4. Seiche Event Observed in Summer 2009

4.1. Cruise Observations

Two years later from the cruise mission of August 2007, a following cruise mission in the SCS deep basin was carried out by Xiamen University, China. The CTD survey with the same instruments and methods as the cruise mission of August 2007 was conducted along the same section 18°N as section *AA* in Figure 1, but at six stations: LE03 (18.00°N 112.00°E), LE04 (17.99°N 113.00°E), LE05 (18.00°N 114.00°E), KK-1 (18.25°N 115.66°E), LE09 (17.99°N 118.00°E), and E406 (18.74°N 120.00°E) from 22 July to 13 August 2009 [*Sun et al.*, 2009]. Figure 7 shows the vertical distribution of the density calculated from cruise-measured temperature and salinity data. One can see the following features. (1) There are systematical oscillation signals along isopycnals. (2) The maximum amplitude (peak-trough) of about 50 m shows on the isopycnal of 27.6 kg m^{-3} located at about 1700 m and centered at 118°N. The amplitudes gradually decrease upward. This seems showing that the initial disturbance source is located at a layer around 1700 m and the disturbance propagates upward only. (3) There are upward peaks centered at around 114 and 118°N, implying that the wavelength of signals is around 400 km.

4.2. Satellite Sea Level Data

Figure 8 shows MADT of the north SCS and the adjacent NPO of 10, 15, 19, and 25 August 2009, partially covering and following the cruise mission from 22 July to 13 August 2009. One can see that similarly to the case of August 2007, a row of three sea level elevation centers E21, E22, and E23 with central sea levels of 10–25 cm higher than the mean sea level was distributed along around 18°N between the mouth of the Gulf of Tonkin and the Luzon Island. The average distance of three eddies is about 380 km. During the observed period from 10 to 25 August 2009, the central positions of three eddies sustained unchanged, namely, they were standing there.

The coherence of three sea level elevation centers E21, E22, and E23 with geostrophic current fields is shown in Figure 9. The curve in Figure 9a represents an SLA transect along 18°N taken from EMD-derived

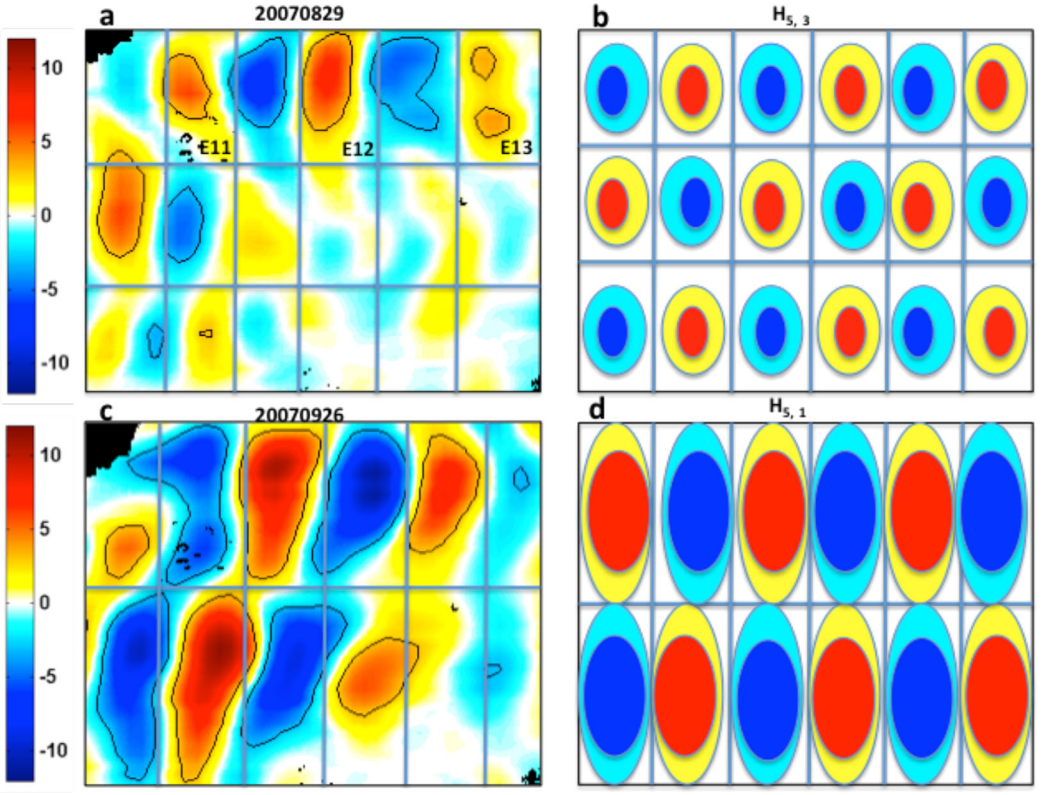

Figure 6. Comparisons of SLA IMF2 derived from the EMD analysis and seiche modes of the model SCS deep basin. (a) Extended seiche event observed by the cruise mission from 20 to 24 August 2007 and (b) a schema of corresponding standing wave mode $H_{5,3}$. (c) The same seiche event but evolving for 4 weeks later and (d) a schema of corresponding standing wave mode $H_{5,1}$. Color codes are in cm in Figures 6a and 6c, and in arbitrary unit in Figures 6b and 6d.

IMF2 of 19 August 2009 derived from of 2-D SLA images, as shown in Figure 10. Figure 9b shows a section of meridional component v of geostrophic current fields along 18°N derived from CTD data measured during the cruise mission of July to August 2009. A 2500 m is selected as a zero level for computing the geostrophic current. One can see very good coherence between the two, i.e., the positive (negative) sea level gradient is corresponding to the positive (negative) meridional geostrophic current. Alternative appearance of the positive and negative currents reveals the wave motion nature of the row of eddies. Vertically, the disturbed depth of the wave motion ($|v| > 0$) reaches deeper than 2000 m, while the strongly disturbed layers ($|v| > 0.05$ m s^{-1}) are concentrated at upper 1000 m.

4.3. Comparison of SLA Patterns to Standing Wave Mode

In order to reconfirm the identity of seiche event observed in July to August 2009 and standing wave mode, we compare 2-D SLA IMF2 in the SCS deep basin (dashed-line rectangle in Figure 10) on 19 August 2009 with theoretical standing wave mode $H_{5,1}$ of a uniformly deep model ocean basin of 1000 by 800 km. As shown in Figure 11, the pattern similarity of Figures 11a and 11b is 75% (9/12). The two images show that the wavelength of standing waves is about 380 km. This case confirms once again that the nature of standing eddy or standing wave phenomena observed in the SCS deep basin is one of intrinsic standing wave or seiche modes.

5. Statistics of Seiche Events in the SCS Deep Basin

In sections 3.3 and 4.2, we have illustrated that the sea level signatures in satellite MADT and SLA images and their EMD-derived IMF images can be used to represent seiche modes of the SCS deep basin, and verified the feasibility to extract the data and information on occurrence, propagation, and evolution of the modes. In this section, we use EMD-derived IMF2 images from 20 years of satellite SLA data from 6 January 1993 to 26 December 2012 for statistical analysis of seiche events occurring in the SCS deep basin.

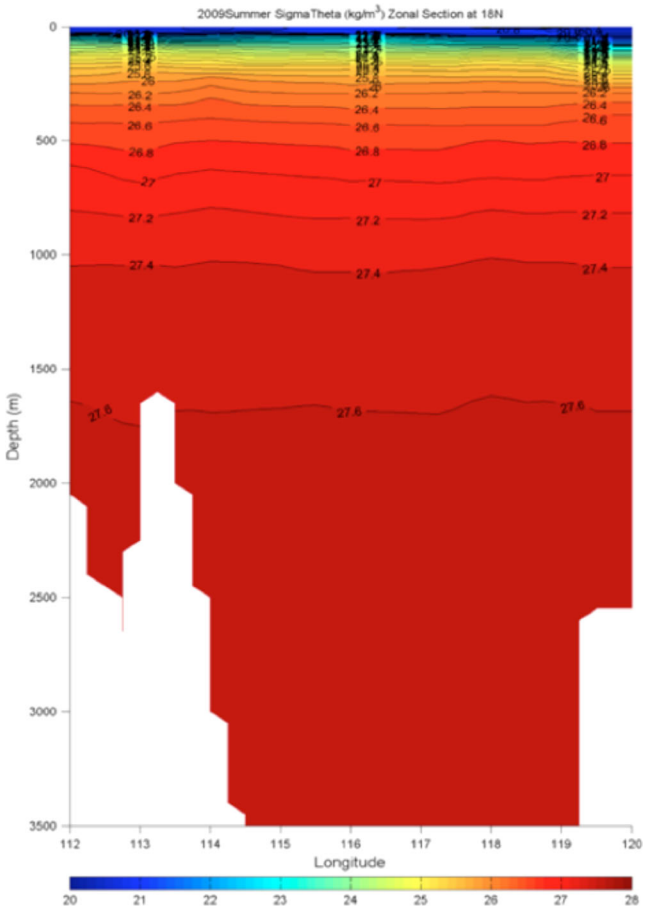

Figure 7. The vertical distribution of the density along section18°N in the SCS deep basin calculated from CTD data measured by the cruise mission of Xiamen University, China, from 22 July to 13 August 2009.

We identify a seiche event by two criteria: (1) amplitudes of alternative positive and negative SLA centers should be larger than 2 cm and (2) standing SLA imagery patterns should last at least for 2 weeks, i.e., the patterns should repeat to appear at least in two sequentially weekly images. Based on the two criteria, we do occurrence statistics for standing wave modes $H_{4,0}$, $H_{5,1}$, and $H_{5,3}$ with the average wavelength ($\bar{\lambda}$) of 500, 390, and 320 km, respectively. The results are listed in Table 2. One can see that during the 20 years (1045 weeks), total 94 events with total temporal coverage of 218 weeks are affirmed. The occurrence frequency increases with mode number: 3.9%, 7.7%, and 9.3% for $H_{4,0}$, $H_{5,1}$, and $H_{5,3}$, implying that seiches of shorter wavelengths occur easier. The total occurrence frequency is 20.9%.

Figure 12 shows histograms of annual and monthly distributions of seiche events and timespans in the SCS deep basin from 1993 to 2012. Figures 12a and 12b show that seiche events might occur in all years with a minimum of two events in 2004 and a maximum of seven events in 1994 and 2001. Meanwhile, histograms of event and timespan show similar interannual variability with a period of about 9 years. In order to clarify possible dependence of seiche events in the SCS on large-scale climate events, we compare the histograms to the Oceanic Niño Index (ONI) time series. We find that the interannual variability shown in histograms seem not to be closely associated with the El Niño and La Niña events, and high event and high timespan years 1993, 1994, 2001, and 2011 were normal years, but 1998 was a strong El Niño year.

On the other hand, histograms of monthly distributions of seiche events and timespans in Figures 12c and 12d show that seiche events may occur in all months in a year with a minimum of two events in December and a maximum of 20 events in October. The two histograms show similar intraseasonal variability with two peaks in May and October, which correspond to the transit periods of local monsoon winds [*Guo et al.*, 2003; *Wang et al.*, 2012].

6. Discussion

6.1. On the Rectangular Basin Model

As shown in Figure 1 and described in section 2, we use a semienclosed rectangular ocean basin with a uniform depth as a model ocean basin to calculate eigen seiche modes. The reasons are twofold. (1) The model is relatively simple and easily solved. (2) The model is a quite good approximation of the SCS deep basin. Examining 94 seiche events derived from satellite altimeter data from 1993 to 2012, we find that in most cases they appeared inside the rectangular basin with borders generally along isobaths of 1000 m as shown in Figures 5 and 10. The real size of the rectangular basin is 1000 km by 800 km as shown in Figure 1. The bottom topography in the rectangular basin is not uniform, but varies from 1000 to 5500 m. However, cruise

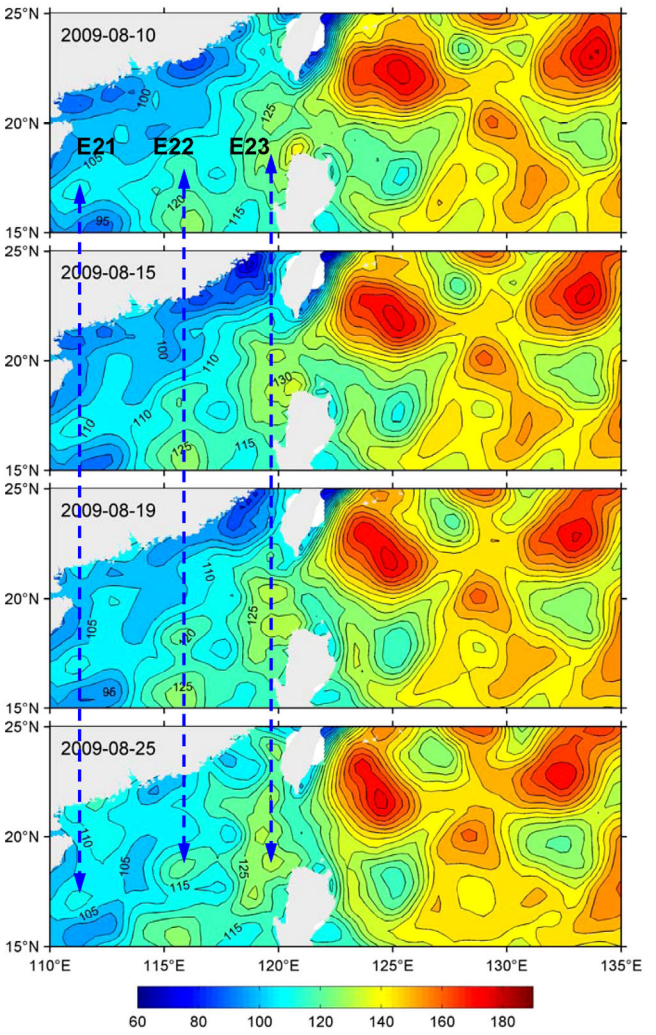

Figure 8. MADT of the north SCS and the adjacent NPO on 10, 15, 19, and 25 August 2009. Three sea level elevation centers E21, E22, and E23 are distributed between 17 and 18°N in the SCS deep basin with the average distance of 380 km. Color codes are absolute sea levels in cm.

observations in summer 2009 as shown in Figure 9 revealed that the strongly disturbed layers of the wave motion ($|v| > 0.05$ m s^{-1}) are concentrated at upper 1000 m, although the disturbed depth ($|v| > 0$) may extend to deeper than 2000 m. This implies that the uniform depth model basin should be a very good approximation of the real SCS deep basin. We use modes $H_{5,1}$ and $H_{5,3}$ derived from the rectangular ocean basin model to explain the seiche events in 2007 and 2009 as shown in Figures 6 and 11. In general, the modeled seiche patterns are comparable to that derived from satellite altimeter data, implying that the physics analysis sounds reasonable. In the case of 2009 (Figures 10 and 11), however, the core locations in the two patterns are not matched well each other. We believe that this may result from modulation of unknown processes to the standing waves, which are worth pursuing in the future research.

6.2. Waves or Eddies

In the above analysis, we have defined a zonal train of alternatively positive and negative SLA centers in the SCS deep basin as the standing wave signatures if the locations of their centers keep unchanged at least for 2 weeks. This is a necessary condition, but not sufficient ones. The sufficient conditions should include that wave peaks would change to wave troughs after half a period. The case of summer 2007 just provided evidence for this polarity switch. From Figures 5 and 6, one can see that on 29 August 2007, the zonal distribution of polarities showed a pattern of N-P-N-P-N-P, and after 4 weeks on 26 September 2007, the pattern changed to P-N-P-N-P-N. In the other words, wave peaks and wave troughs had switched each other. From here, we estimate that the period of the standing waves is of the order of 60 days, which will further be discussed in section 6.3.

From the point of view of oscillation theory, an intrinsic standing wave mode represents a stable state of the basin. From Table 2, one can see that the occurrence frequency and timespan of each mode in the SCS vary and look random. For example, in the case of summer 2007, the timespan of mode $H_{5,3}$ was as long as 4 weeks from 5 to 29 August 2007 (Figures 3 and 5a), while in the case of September 2007, the timespan of mode $H_{5,1}$ was about 2 weeks only from 26 September to 3 October 2007 (Figures 5b and 6c). This implies that the stable state is critical and fragile. Besides the polarity change, other dynamical processes, such as changes in the initial disturbance and the background circulation system, may also destroy the stable state. As the stable state is destroyed, the standing waves transforms to the traveling waves, which will propagate southwestward with the phase speed of the first baroclinic Rossby wave mode [*Cai et al.*, 2008; *Wang et al.*, 2008; *Nan et al.*, 2011].

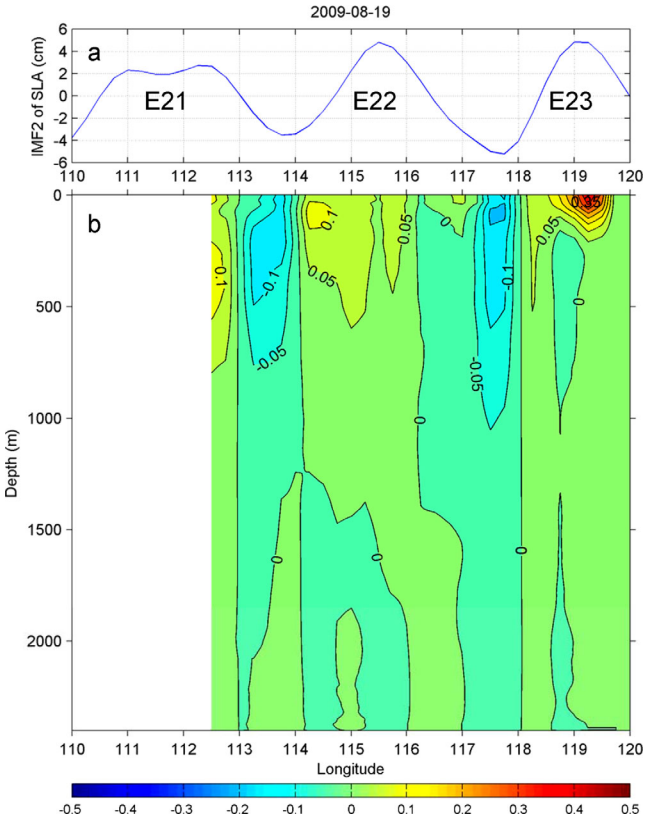

Figure 9. Coherence of three sea level elevation centers E21, E22, and E23 with the meridional component of geostrophic current fields derived from the CTD data during the cruise mission of July to August 2009.

It is worth noting that as a whole, the standing sea level elevation and depression centers constitute a wave packet. On the other hand, for an individual SLA center, dynamical balance requires its cyclonical or anticyclonical rotation motion to maintain the negative or positive SLA. Thus the individual SLA center behaves as an eddy, and the whole wave packet behaves as an alternatively cyclonical and anticyclonical eddy train. In the two cases analyzed in this study, the geostrophic current fields derived from cruise measurements, shown in *Nan et al.* [2011, Figure 5] and Figure 9 in this paper, verify that it is true. The previous observations and numerical simulations have also evidenced this phenomenon [*Chu et al.*, 1998; *Wang et al.*, 2004; *Hu et al.*, 2012].

6.3. On Disturbance Sources

The cruise observations in summer 2007 (Figure 2) and summer 2009 (Figure 7) revealed that the initial disturbance of seiche events came from depths of 500–700 m and 1500–1700 m, respectively. In other words, the seiche events were initially generated in the two layers. Checking the SCS bottom topography in Figure 1, one can see that at such depths the Luzon Strait is an only waterway still connecting the NPO with the SCS. Thus it seems reasonable to imagine that the initial disturbance of seiche events observed in the SCS originates from the NPO.

As mentioned in section 3.4, standing wave modes of the SCS deep basin may occur at specific frequencies or wavelengths. The three standing sea level elevation centers in Figure 3 represent an internal standing wave train with an average wavelength of about 320 km. On the other hand, we have extracted sea level signatures of corresponding 320 km band (IMF2) from SLA data from 6 January 1993 to 26 December 2012 using the EMD method. In order to examine the propagation and evolution of IMF2 from the NPO to the SCS, we show its longitude-time plot from 107°E to 135°E along 20°N, where is the zonal central line of the Luzon Strait, for the first 5 years from 1993 to 1998 in Figure 13. One can see that the propagation patterns of IFM2 can be divided

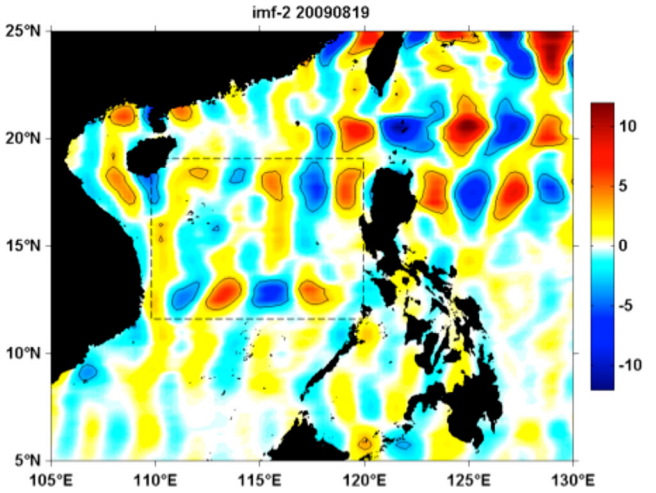

Figure 10. Same as Figure 5, but on 19 August 2009.

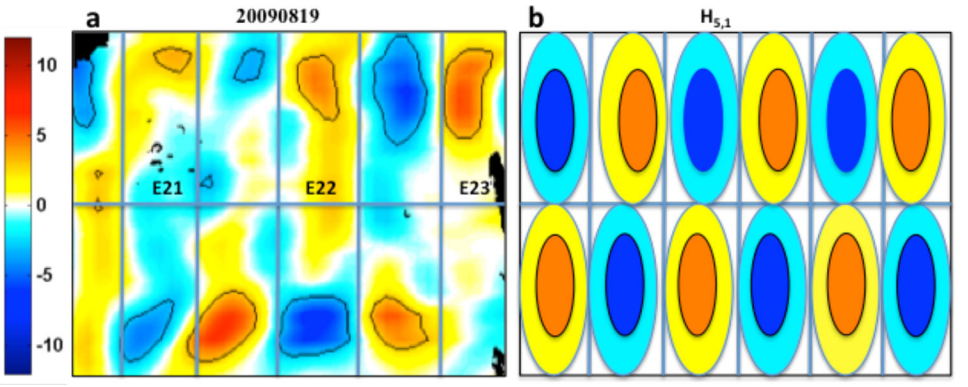

Figure 11. (a and b) The same as Figures 6c and 6d, but for the cruise mission of July to August 2009.

into two zones with a boundary at 123°E, zones 21 and 22. Between the two zones there are no a shadow zone, implying that IMF2 penetrates the LS and enters the SCS directly. Zone 21 is located on the east side, where is the NPO water. The mode shows a westward traveling wave pattern, implying that IMF2 serves as

Table 2. Statistics of Seiche Events in the SCS Deep Basin From 6 January 1993 to 26 December 2012 (1045 Weeks)

Seiche Mode	$H_{4,0}$ $\bar{\lambda}$: 500 km	$H_{5,1}$ $\bar{\lambda}$: 390 km	$H_{5,3}$ $\bar{\lambda}$: 320 km
Dates of events	9/29-10/6 1993	2/3-2/10 1993	1/6-1/20 1993
	6/22-7/6 1994	3/24-3/31 1993	6/9-6/16 1993
	9/14-9/21 1994	7/7-7/14 1993	3/30-4/6 1994
	9/6–9/13 1995	10/26-11/2 1994	5/11-5/25 1994
	2/12-2/26 1997	9/27-10/4 1995	8/31-9/7 1994
	10/28-11/4 1998	8/28-9/4 1996	9/21-10/5 1994
	3/3-3/10 1999	1/8-1/22 1997	5/31-6/7 1995
	9/20-10/11 2000	4/9-4/16 1997	5/29-6/5 1996
	10/17-10/31 2001	5/28-6/4 1997	7/3–7/10 1996
	11/20-11/27 2002	1/28-2/4 1998	11/6–11/13 1996
	11/30-12/7 2005	5/13-5/20 1998	3/12-3/19 1997
	8/30-9/6 2006	2/3-2/10 1999	2/25-3/4 1998
	11/5–11/12 2008	4/14-5/5 1999	7/29-8/26 1998
	2/17-3/10 2010	5/24-6/7 2000	10/7–10/21 1998
	5/26-6/2 2010	3/7-3/14 2001	1/13-1/20 1999
	9/28-10/5 2011	4/18-4/25 2001	6/30-7/21 1999
	10/10-10/17 2012	5/30-6/6 2001	9/13-10/11 2000
		8/8-8/15 2001	11/29-12/6 2000
		11/14-11/28 2001	5/23-5/30 2001
		3/20-3/27 2002	5/1–5/8 2002
		5/29-6/5 2002	11/13-11/20 2002
		9/24-10/1 2003	4/9-4/16 2003
		3/24-3/31 2004	4/30-5/7 2003
		9/22-9/29 2004	10/22-10/29 2003
		10/26-11/2 2005	2/23-3/2 2005
		9/20-9/27 2006	11/9–11/16 2005
		10/11-10/18 2006	5/10-5/17 2006
		6/27-7/4 2007	1/31-2/7 2007
		9/26-10/3 2007	8/5–8/29 2007
		7/9-7/16 2008	10/17-10/24 2007
		10/15-10/22 2008	8/13-8/20 2008
		7/15-7/29 2009	6/3–6/10 2009
		8/19-8/26 2009	8/19-8/26 2009
		9/23-9/30 2009	4/14-4/21 2010
		3/2–3/9 2011	5/26-6/2 2010
		10/6–11/2 2011	4/27-5/4 2011
			6/22-6/29 2011
			2/1–2/8 2012
			3/21-3/28 2012
			8/1–8/8 2012
			10/17-10/24 2012
Total events	17	36	41
Total temporal coverage (weeks)	41	80	97
Occurrence frequency	3.9%	7.7%	9.3%

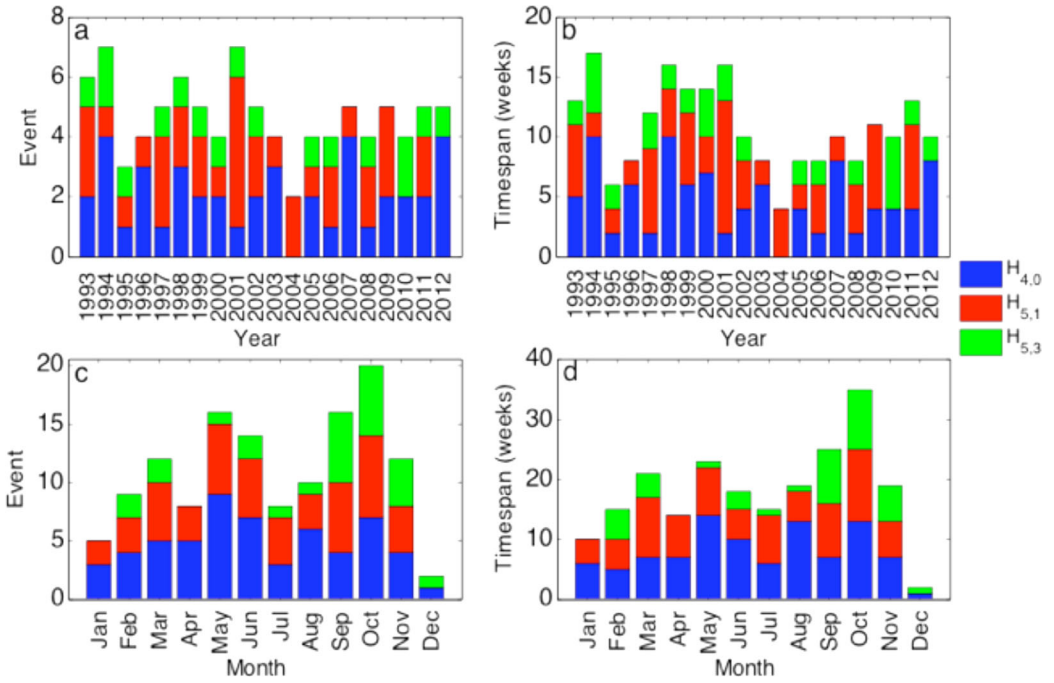

Figure 12. Histograms of (a and c) annual and monthly distributions of seiche events and (b and d) timespans in the SCS deep basin from 1993 to 2012. Blue, red, and green bars represent seiche modes $H_{4,0}$, $H_{5,1}$, and $H_{5,3}$, respectively.

an incident wave from the NPO to the Luzon Strait. The average period is 2.5 months (75 days), and the average phase speed is 8 cm s^{-1}. Zone 22 is located on the west side of the boundary, where includes the Luzon Strait and the SCS. The mode shows interference wave patterns. In particularly, the SCS west of 120°E shows standing wave patterns at most of time, i.e., the iso-phase lines are generally parallel to the horizontal axis. Meanwhile, the average period is shortened to 2.0 months (60 days). This value agrees with that estimated by the switch time of wave peaks and wave troughs in the case of summer 2007 obtained in section 6.2.

On the other hand, we can use equation (3) to estimate the periods of internal seiche modes. In this case, equation (3) should be rewritten as

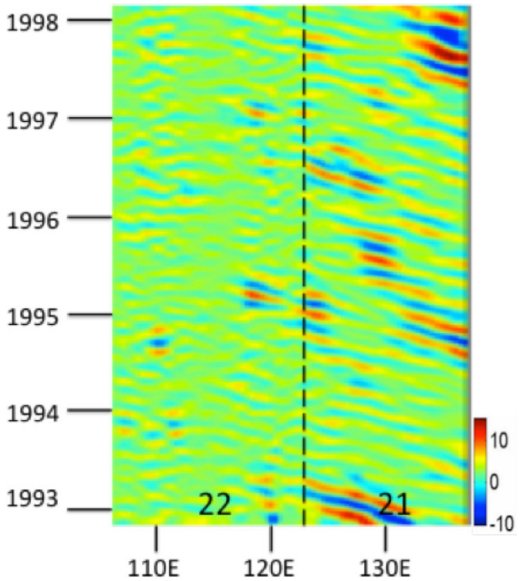

Figure 13. Longitude-time plots of IMF2 from 107°E to 135°E along 20°N and from 1993 to 1998. The vertical dash line is 123°E near the eastern boundary of the Luzon Strait. Color codes are SLA in cm.

$$T_{mn} = \frac{2}{\sqrt{g' H'}} \left[\left(\frac{m}{L}\right)^2 + \left(\frac{n}{l}\right)^2 \right]^{-1/2}, \quad (5)$$

where $g'\left(=\frac{\delta\rho}{\rho}g\right)$ is a reduced gravitational acceleration, and H' is the amplitude of the seiche mode. From Figure 7, one can see that at layer of 1700 m, H' is about 50 m and $\delta\rho/\rho$ is about 1 $\times 10^{-5}$. Substituting these values and the values of L and l of the rectangular model SCS deep basin yields $T_{5,1}$ and $T_{5,3}$ as 64 and 53 days, respectively, which are close to that derived from Figure 13. This implies a resonant process between the SCS deep basin and the disturbance originating from the NPO. From

Figures 5a and 5b, one can see that the amplitudes of sea level elevation and depression centers are not uniformly distributed in the basin, but strong in north and west basin and weak in south and east basin. This seems associated with the path of SCS Throughflow originating from the NPO [*Fang et al*., 2005; *Zheng et al*., 2006].

7. Conclusions

This study deals with standing wave or seiche events in the SCS deep basin using theoretical analysis, cruise observations along 18°N in summer 2007 and 2009 as well as satellite altimeter data products from 1993 to 2012. Major findings are summarized as follows.

1. Using a rectangular ocean basin with a uniform depth, a west-east length of 1000 km and a north-south width of 800 km as a model of the SCS deep basin, we calculate the eigen wavelengths of seiche modes. Modes $H_{5,3}$ and $H_{5,1}$ are used to explain the SLA signatures of seiche events observed in summer 2007 and 2009. The similarity between the two is higher than 75%.

2. A cruise mission in summer 2007 and a repeated mission in summer 2009 detected internal oscillation signals along section 18°N in the SCS deep basin with average wavelengths of about 320 and 390 km. The maximum disturbance signals were located at layers 500–700 m and 1500–1700 m, respectively. Simultaneous satellite altimeter SLA images and their EMD-derived IMF2 show that the observed internal oscillations are a portion of 2-D standing wave patterns, which lasted for at least 2 weeks. We further recognize that the observed internal oscillation signals represent seiche modes of the SCS deep basin $H_{5,3}$ and $H_{5,1}$.

3. This study confirms that the sea level signatures in satellite MADT and SLA images and their EMD-derived IMF images are highly coherent with seiche modes of the SCS deep basin. Thus we use EMD-derived IMF2 images from 1993 to 2012 for statistical analysis of seiche modes $H_{4,0}$, $H_{5,1}$, and $H_{5,3}$ with average wavelength $\bar{\lambda}$ of 500, 390, and 320 km. The results indicate that during the 20 years (1045 weeks), total 94 events with total temporal coverage of 218 weeks are affirmed. The total occurrence frequency is 20.9%. Histograms of annual distributions of seiche events and timespans show that seiche events might occur in all years with an interannual variability of about 9 years. The interannual variability seems not to be closely associated with the El Niño and La Niña events. High event and high timespan years 1993, 1994, 2001, and 2011 were normal years, but 1998 was a strong El Niño year. Histograms of monthly distributions of seiche events and timespans show that seiche events may occur in all months in a year with an intraseasonal variability double-peaked in May and October, which are the transit periods of East Asia monsoon in the SCS [*Guo et al*., 2003; *Wang et al*., 2012]. Physics behind the statistical results need to be further clarified.

Acknowledgments

The satellite altimeter data for this paper are available at Archiving Validation and Interpretation of Satellite Data in Oceanography (AVISO), the Centre National d'Études Spatiales (CNES) of France (http://www.aviso.altimetry.fr/en/data/products/sea-surface-height-products/global.html). This work is supported by the US National Science Foundation award AGS-1061998 (for Zheng) and the Natural Science Foundation of China project 41276006. We are grateful to three anonymous reviewers for their valuable suggestions and comments for improving the manuscript.

References

Cai, S., X. Long, R. Wu, and S. Wang (2008), Geographical and monthly variability of the first baroclinic Rossby radius of deformation in the South China Sea, *J. Mar. Syst.*, *74*, 711–720.

Cai, S., J. Xie, and J. He (2012), An overview of internal solitary waves in the South China Sea, *Surv. Geophys.*, *33*, 927–943.

Cao, C., K. Guo, K. Li, and Z. Chen (2001), Synoptic analyses for the formation of large-amplitude seiche in the main harbors along the coasts of the Bohai Sea and Huanghai Sea, *Atca Oceanol. Sin.*, *23*(5), 24–32.

Chu, P. C., Y. Chen, and S. Lu (1998), Wind-driven South China Sea deep basin warm-core/cool-core eddies, *J. Oceanogr.*, *54*, 347–360.

Fang, G., D. Susanto, I. Soesilo, Q. Zheng, F. Qiao, and Z. Wei (2005), A note on the South China Sea shallow interocean circulation, *Adv. Atmos. Sci.*, *22*, 946–954.

Giese, G. S., and R. B. Hollander (1987), The relation between coastal seiches at Palawan Island and tide-generated internal waves in the Sulu Sea, *J. Geophys. Res.*, *92*, 5151–5156.

Guo, X., C. Jing, and L. Li (2003), Wind field features in Nansha Islands waters, Southern South China Sea—Satellite scatterometer data analysis, *J. Trop. Oceanogr.*, *22*, 18–25.

Hu, J., H. Kawamura, H. Hong, F. Kobashi, and D. Wang (2001), 3∼6 months variation of sea surface height in the South China Sea and its adjacent ocean, *J. Oceanogr.*, *57*, 69–78.

Hu, J., J. Gan, Z. Sun, J. Zhu, and M. Dai (2011), Observed three-dimensional structure of a cold eddy in the southwestern South China Sea, *J. Geophys. Res.*, *116*, C05016, doi:10.1029/2010JC006810.

Hu, J., Q. Zheng, Z. Sun, and C.-K. Tai (2012), Penetration of nonlinear Rossby eddies into South China Sea evidenced by cruise data, *J. Geophys. Res.*, *117*, C03010, doi:10.1029/2011JC007525.

Huang, N. E., Z. Shen, S. R. Long, M. C. Wu, H. H. Shih, Q. Zheng, N.-C. Yen, C. C. Tung, and H. H. Liu (1998), The empirical mode decomposition and the Hilbert spectrum for nonlinear and non-stationary time series analysis, *Proc. R. Soc. London, Ser. A*, *454*, 903–995.

Jia, Y., and Q. Liu (2004), Eddy shedding from the Kuroshio bend at Luzon Strait, *J. Oceanogr.*, *60*, 1063–1069.

Lamb, H. (1945), *Hydrodynamics*, 6th ed., pp. 1–738, Dover, N. Y.

Li, L., W. D. Nowlin Jr., and J. Su (1998), Anticyclonic rings from the Kuroshio in the South China Sea, *Deep Sea Res., Part I*, *45*, 1469–1482.

Lin, H., J. Hu, and Q. Zheng (2012), Satellite altimeter data analysis of the South China Sea and the northwest Pacific Ocean: Statistical features of oceanic mesoscale eddies, *J. Oceanogr. Taiwan Strait*, *30*, 105–113.
Mei, C. C. (1992), *The Applied Dynamics of Ocean Surface Waves*, pp. 1–740, World Sci., London, U. K.
Metzger, E. J., and H. E. Hurlburt (2001), The nondeterministic nature of Kuroshio penetration and eddy shedding in the South China Sea, *J. Phys. Oceanogr.*, *31*, 1712–1732.
Metzner, M., M. Gade, I. Hennings, and A. B. Rabinovich (2000), The observation of seiches in the Baltic Sea using a multi data set of water levels, *J. Mar. Syst.*, *24*, 67–84.
Münnich, M., A. Wüest, and D. M. Imboden (1992), Observations of the second vertical mode of the internal seiche in an alpine lake, *Limnol. Oceanogr.*, *37*, 1705–1719.
Nan, F., Z. He, H. Zhou, and D. Wang (2011), Three long-lived anticyclonic eddies in the northern South China Sea, *J. Geophys. Res.*, *116*, C05002, doi:10.1029/2010JC006790.
Rabinovich, A. B. (2009), Seiches and harbor oscillations, in *Handbook of Coastal and Ocean Engineering*, edited by Y. C. Kim, chap. 6, pp. 193–236, World Sci., Singapore.
Raichlen, H. (1966), Harbor resonance, in *Estuary and Coastline Hydrodynamics*, edited by A. T. Ippen, pp. 281–340, McGraw Hill, N. Y.
Ramp, S. R., T. Y. Tang, T. F. Duda, J. F. Lynch, A. K. Liu, C.-S. Chiu, F. L. Bahr, H.-R. Kim, and Y.-J. Yang (2004), Internal solitons in the Northeastern South China Sea Part I: Sources and deep water propagation, *IEEE J. Oceanic Eng.*, *29*, 1157–1181.
Sun, Z., F. Tao, Z. Wu, J. Zhu, J. Hu, and M. Dai (2009), Temperature and salinity data report: CHOICE-C cruise in the South China Sea in summer 2009, *Tech. Rep. CMI-031*, pp. 273, Xiamen University, Xiamen.
Toshiyuki, H., and K. Kajiura (1982), Origin of 'Abiki' phenomenon (kind of seiches) in Nagasaki Bay, *J. Oceanogr. Soc. Jpn.*, *38*, 172–182.
Vilibić, I., and H. Mihanović (2003), A study of resonant oscillations in the Split harbor (Adriatic Sea), *Estuarine Coastal Shelf Sci.*, *56*, 861–867.
Wang, D., H. Xu, J. Lin, and J. Hu (2008), Anticyclonic eddies in the northeastern South China Sea during winter 2003/2004, *J. Oceanogr.*, *64*, 925–936.
Wang, G., J. Su, and P. Chu (2003), Mesoscale eddies in the South China Sea observed with altimeter data, *Geophys. Res. Lett.*, *30*(21), 2121, doi:10.1029/2003GL018532.
Wang, H., Y. Yuan, W. Guan, R. Lou, and K. Wang (2004), Circulation in the South China Sea during summer 2000 as obtained from observations and a generalized topography-following ocean model, *J. Geophys. Res.*, *109*, C07007, doi:10.1029/2003JC002134.
Wang, H., C. Wang, J. Xiang, J. Li, and C. Liu (2012), Validation of QuikSCAT satellite scatterometer winds and characteristics of monthly mean wind speed in South China Sea, *J. Meter. Sci.*, *33*, 1–7.
Wang, J., and C.-S. Chern (1987), The warm-core eddy in the northern South China Sea I. Preliminary observations on the warm-core eddy, *Acta Oceanogr. Taiwan.*, *18*, 92–103.
White, W. B., and J. F. T. Saur (1981), A source of annual baroclinic waves in the eastern subtropical North Pacific, *J. Phys. Oceanogr.*, *11*, 1452–1462.
Wilson, B. (1972), Seiches, *Adv. Hydrosci.*, *8*, 1–94.
Wüest, A., and D. M. Farmer (2003), Seiche, in *McGraw-Hill Encyclopedia of Science & Technology*, 9th ed., pp. 1–8, McGraw-Hill, N. Y.
Xia, Z., S. Lin, Y. Wang, S. Mai, and J. Zhang (2002), Seiches at the coastal stations along the north coast of South China Sea, *Chin. J. Oceanol. Limnol.*, *1*, 8–14.
Xie, L., J. Tian, S. Zhang, Y. Zhang, and Q. Yang (2011), An anticyclonic eddy in the intermediate layer of the Luzon Strait in autumn 2005, *J. Oceanogr.*, *67*, 37–46, doi:10.1007/s10872-011-0004-9.
Xiu, P., F. Chai, L. Shi, H. Xue, and Y. Chao (2010), A census of eddy activities in the South China Sea during 1993–2007, *J. Geophys. Res.*, *115*, C03021, doi:10.1029/2009JC005657.
Zheng, Q., G. Fang, and Y. T. Song (2006), Introduction to special section: Dynamic processes and circulation in Yellow Sea, East China Sea, and South China Sea, *J. Geophys. Res.*, *111*, C11S01, doi:10.1029/2005JC003261.
Zheng, Q., R. D. Susanto, C.-R. Ho, Y. Tony Song, and Qing Xu (2007), Statistical and dynamical analyses of generation mechanisms of solitary internal waves in the northern South China Sea, *J. Geophys. Res.*, *112*, C03021, doi:10.1029/2006JC003551.
Zheng, Q., H. Lin, J. Meng, X. Hu, Y. T. Song, Y. Zhang, and C. Li (2008a), Sub-mesoscale ocean vortex trains in the Luzon Strait, *J. Geophys. Res.*, *113*, C04032, doi:10.1029/2007JC004362.
Zheng, Q., Y. T. Song, H. Lin, X. Hu, J. Meng, and D. Wang (2008b), On generation source sites of internal waves in the Luzon Strait, *Atca Oceanol. Sin.*, *27*, 38–50.
Zheng, Q., C.-K. Tai, J. Hu, H. Lin, R. Zhang, F.-C. Su, and X. Yang (2011), Satellite altimeter observations of nonlinear Rossby eddy–Kuroshio interaction at the Luzon Strait, *J. Oceanogr.*, *67*, 365–376, doi:10.1007/s10872-011-0035-2.